Int. Journ. of Laser Science, Vol. 1, pp. 185–205
Reprints available directly from the publisher
Photocopying permitted by license only

Numerical Analysis of Laser-assisted Ti to Polyimide Welding Using a Statistical Approach

M.S. SHAIKH MOHAMMAD MEIABADI[1], A. KAZAROONI AND M. MORADI[2,3,*]

[1]*Department of Mechanical Engineering, Faculty of Engineering, SRTT University, Tehran, Iran*
[2]*Department of Mechanical Engineering, Faculty of Engineering, Malayer University, Malayer, Iran*
[3]*Laser Materials Processing Research Center, Malayer University, Malayer, Iran*

Many efforts have been made at attaining direct joint between metals and polymers. Laser welding of dissimilar materials is a promising method to bond metals and polymers. In this study, we have developed a finite element (FE) model using ABAQUS software to investigate thermal phenomena of the laser welding of Ti to polyimide. Cylindrical-involution-normal (CIN) heat source model is used to describe heat source power distribution. The Fortran software is used to programme the CIN heat source model and is linked to ABAQUS. The validation of the FE model is confirmed by attaining the analogous results to experimental data. The design of experiments (DOE) approach is utilized to statistical analysis of laser welding of Ti to polyimide. The effects of laser power (0.5 to 1.5 W) and laser scanning speed (50 to 150 mm/min) on average bond width and delta bond width have been investigated *via* response surface methodology (RSM). The analysis is designed based on central composite design (CCD) full replication with two factors five levels. Results reveal that laser power is the most significant variable on average bond width and the laser scanning speed is the most influential variable on delta bond width.

Keywords: Laser welding, titanium, Ti, polyimide, numerical analysis, ABAQUS, Fortran, finite element (FE), central composite design (CCD), response surface methodology (RSM)

*Corresponding author: Tel: +98 (0)81 3222 5312 8; E-mail: moradi@malayeru.ac.ir

1 INTRODUCTION

Combination of light metals and thermoplastics in integrated systems is increasing because of rising trend in producing systems with special mechanical, physical and thermal properties; hence, light metals and thermoplastics are being used as complementary elements in integrated systems due to their compatible properties in various industries. So, the joining methods of dissimilar materials is of great importance in combinational systems like microelectromechanical systems.

Generally, methods to join metals with thermoplastics can be divided in in-mould assembly (IMA) and post-mould assembly (PMA). IMA is feasible for the plastic injection moulded parts with special geometry which surround the metal part and is always accompanied by technical difficulties. PMA entails several mechanical joining processes, adhesive bonding and thermal joining. Application of heavy components like bolts and rivets in the mechanical joining of lightweight structures is not favourable and also is impossible in tiny systems; furthermore, drilling processes, which are inevitable for bolt and rivet joints, lead to stress concentration and also unbalanced load distribution. Aerospace and automotive industries are always in pursuit of reducing weight of structures for compelling reasons; namely, boosting the performance of their vehicles. Automotive industries should reduce fuel consumption to reduce emission of CO_2 to address environmental problems. On the other hand, using conventional joining techniques toward medical applications is fairly impossible due to corrosive environment and small size of joining parts. Adhesive bonding is more suitable for large area joining parts [1] and also these joints suffer from sudden fracture which raises safety concerns; moreover, adhesives mostly contain harmful materials which limit their applications in medical equipment.

Laser materials processing is recently used for various engineering applications; cutting [2], drilling [3], welding [4, 5] and brazing [6]. Laser welding has received great attention due to high quality, high precision, high performance, high speed, good flexibility and low deformation or distortion [7]. Laser welding of dissimilar materials is a promising solution for joining difficulties in various applications ranging from industrial structures to medical devices [8]. Laser welding is able to solve the problems of typical polymer-metal joining technologies, like screwing, riveting and adhesives [9].

S. Katayama *et al.* [10] focused on the fundamentals of the formation mechanism of strong laser direct joints between polyethylene terephthalate (PET) plastic and 304 stainless steel. These 30 mm wide metal-plastic joints possess high tensile shear loads of more than 1.2 kN. Transmission electron microscope (TEM) micrographs of the joint demonstrated that 304 stainless steel and the PET were bonded on the atomic, molecular or nanostructural level through a Cr oxide film. Dhorajiya *et al.* [11] developed a comprehensive three-dimensional (3-D) transient model for sequentially coupled thermal/mechanical analysis of transmission laser (laser beam with wavelength of 1100 nm and diameter of 0.2 mm) microjoining of two dissimilar materials by using the finite element (FE) code ABAQUS along with a moving Gaussian laser heat source.

Wahbaa *et al.* [12] produced lap joints between AZ91D thixomolded Mg alloy and PET by direct irradiation of high power diode laser beam from either plastic or metal side [12]. Hino *et al.* [13] studied laser joining for different materials between 1050 Al-alloy sheet of 1 mm thickness and polypropylene (PP) sheet of 2 mm thickness using a newly developed insert sheet. The effects of the Al surface state on the joining properties were examined [13]. Kawahitoa *et al.* [14] applied the laser-assisted metal to polymer (LAMP) welding method to join Si3N4 and PET, although metal was replaced by ceramic. The joints produced with a linear shape of a diode laser beam were evaluated by the tensile shear test [14].

Roesnera *et al.* [15] used laser radiation to ablate the metal surface in order to create microstructures with undercut grooves to overcome the problems of state-of-the-art joining dissimilar materials technologies. By using a microstructure with an undercut shape, the mechanical interlock of the joint is established and high shear strengths up to 24 MPa can be achieved [15]. Sano *et al.* [16] succeeded in directly joining Cu with PET using femtosecond laser pulses, which were focused through PET onto the Cu surface which was thermally adhered to PET prior to the laser irradiation. They suggested that the ultrashort pulse width of the laser enables the direct joining of these dissimilar materials, thereby avoiding graphitization of the polymeric material. Heckert *et al.* [17] pre-treated Al sheets with laser radiation; subsequently, the specimens were joined to glass fibre reinforced titanium posts (TP), with different fibre length and fibre content, by laser-based heat conduction joining. They demonstrated that with laser surface pre-treatment high joint strengths are obtained. Markovitsa *et al.* [18] joined poly (methyl methacrylate) (PMMA) to structural steel by adhesives and by LAMP joining. Mechanical tests were carried out to compare the two different technologies, and to be able to position the LAMP joining within the field of joining technologies. Results show clearly the advantages of laser transmission joining as compared to adhesives. Lamberti *et al.* [19] reported a novel laser beam joining process for hybrid polyamide-Al structures. They optimized the spatial and temporal heat input for optimal bonding quality. It was shown that laser or electro-chemical surface pre-treatment of the Al substrate has a distinctive effect on the shear strength of the joint.

Vidal *et al.* [20] reported a novel combined experimental and numerical approach to laser joining of hybrid polymer-metal parts. Experiments on conductive laser joining of glass reinforced polyamide to steel for different metal pre-treatment conditions were performed. The selection of parameters for the joining process was assisted by a FE modelling, which is able to provide the parameter window for appropriate interface temperature with good accuracy, and thus, reduce notably the need for trial and error experiments. Schricker *et al.* [21] analysed the melting layer in thermal joining of polymer-metal hybrid joints according to process management and microstructure. Preliminary investigations provided results on line joints regarding the melting layer and microstructure which were transferred to spot joints as a model concept to avoid process uncertainties and heat accumulation.

Altogether, the direct laser joining of hybrid parts is still in a development stage for industrial use and a deeper research have to be carried out in order to improve the mechanical performance of the produced assemblies [22]. In microelectronics the presence of moisture and other contaminants may lead to chemical attack of the chip metallization or can alter the electrical characteristics of the device. The challenges in the packaging of such systems result from the small size of the features and the localized joining of the different materials. Typical materials used in these devices include metals such as Ti and polymers such as polyimide, whose biocompatibility is already proven [23].

In this study laser-assisted Ti to polyamide welding process is investigated. A FE model is developed to simulate laser welding of Ti to polyamide by ABAQUS software. Cylindrical-involution-normal (CIN) is utilized to describe heat source power distribution in laser-assisted metal to polymer welding. The heat source model is programmed by the Fortran software. The FE model is validated by experimental results of the laser welding process. The FE model is precisely capable of predicting temperature distribution of welding process in the materials which primarily determines bond width. In addition, effects of laser power and laser scanning speed on the bond width variation are evaluated by FE model. Response surface methodology (RSM) is used to carry out statistical analysis and clearly determines effects of laser power and laser scanning speed and their interactions on the bond width along with laser travelling direction.

2 LASER TRANSMISSION JOINING

The direct laser transmission joining is a rapid, flexible and reliable solution to bond the entire surfaces of two dissimilar materials without any adhesive or mechanical joint. In transmission joining the laser beam is transmitted through the plastic material and heats the metal joining partner; consequently, the temperature of the metal plastic interface rises until the plastic is molten. This process can only be applied to plastics which show a high level of transparency for electromagnetic radiation of the laser wavelength.

Activated high temperature plastic melt which is in contact with the laser heated metal surface undergoes high pressure caused by the generation and rapid expansion of bubbles, and consequently physical or chemical bonding between the metal and the plastic is achieved. The strong joint could be produced by atomic, nanostructural or molecular bonding of the metal and the plastic through the oxide film on the metal plate surface, where not only the anchor (mechanical bonding) effect but also Van der Waals interaction forces and chemical bonding were expected [7, 10, 12, 14]. A schematic diagram of the laser transmission joining of Ti and polyimide is shown in Figure 1.

3 MATHEMATICAL AND NUMERICAL DESCRIPTION

3.1 Heat source description

A very important issue in the modelling of welding processes is an appropriate selection of the heat source power distribution, primarily responsible for the melted pool shape and the temperature distribution in the material [24]. Energy absorption in the laser welding and the immediate transport of the heat below the surface of the workpiece is determined by two mechanisms of Fresnel's absorption and inverse Bremsstrahlung's absorption [25]. In numerical modelling of laser beam welding process Gaussian distribution of the heat source is usually assumed in radial direction [26]. A good approximation of volumetric heat source power distribution, Q, is given in universal CIN heat source model [27]:

$$Q(r,z) = \frac{kK_z\eta_L Q_L}{\pi\left(1-e^{\left(K_z s\right)}\right)} e^{-\left(kr^2+K_z z\right)}\left[1-u\left(z-s\right)\right] \tag{1}$$

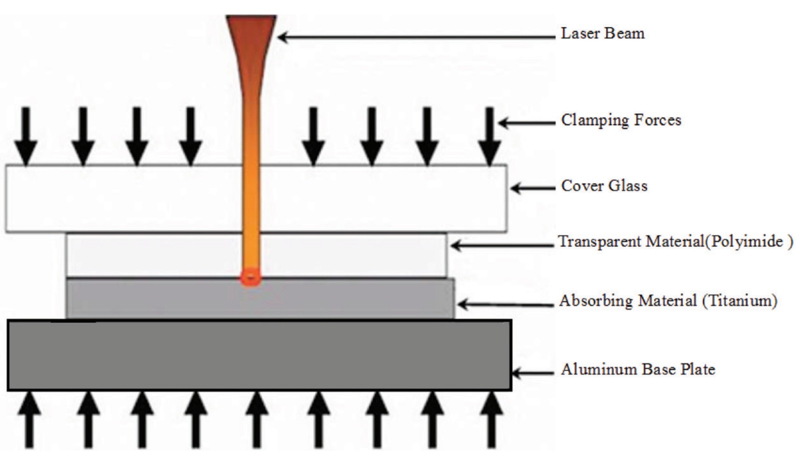

FIGURE 1
Schematic diagram of the transmission laser joining of Ti and polyimide.

where Q_L is the laser beam power, η_L is a laser efficiency, $K_Z=3/s$ is a heat source power exponent, r_0 is a beam radius, $k=3/r_0^2$ is a beam focus coefficient and s is the heat source beam penetration depth, $u(z\text{-}s)$ is the Heaviside function. The CIN heat source power distribution is shown in Figure 2. The Fortran software is used to programme the CIN heat source model.

3.2 Governing equations

In this work, heat transfer modes include conduction in Ti, polyamide, Al and glass, natural convection and radiation to surrounding in all components, and gap conduction and radiation between Ti and polyamide. For uniform and continuous media, the spatial and temporal temperature distribution $T(x,y,z,t)$ satisfies the following differential equation for 3-D heat conduction in a domain D:

$$\frac{\partial}{\partial x}\left(k_x(T)\frac{\partial T}{\partial x}\right)+\frac{\partial}{\partial y}\left(k_y(T)\frac{\partial T}{\partial y}\right)+\frac{\partial}{\partial z}\left(k_z(T)\frac{\partial T}{\partial z}\right)+Q=\rho c\left(\frac{\partial T}{\partial t}-v\frac{\partial T}{\partial y}\right) \tag{2}$$

where x, y, z are the coordinate values of the Cartesian coordinate system; T is the temperature; t is the time; ρ is the material density; c is the specific heat

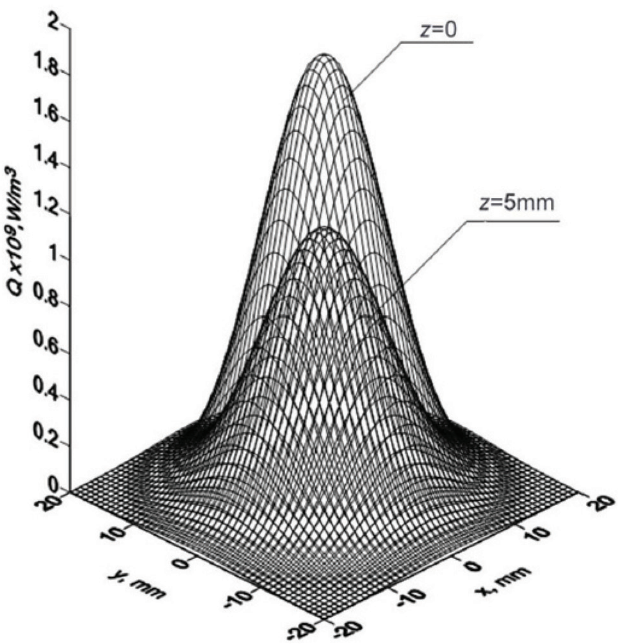

FIGURE 2
CIN heat source power distribution [24].

capacity; k_x, k_y, k_z are the thermal conductivities in the x-, y- and z-directions, respectively; and v is the velocity of laser beam traversing across the surface. The initial condition can be written as

$$T = \left(x, y, z, 0\right) = T_0 \quad \text{for} \quad \left(x, y, z\right) \in D \tag{3}$$

The natural boundary condition can be defined as

$$k_n \frac{\partial T}{\partial n} - q + h\left(T - T_0\right) + \sigma\varepsilon\left(T^4 - T_0^4\right) = 0 \quad \text{for} \quad \left(x, y, z\right) \in S \tag{4}$$

where k_n denotes the thermal conductivity at each node, q denotes the experimentally determined heat flux normal to S, h_{conv} is the convection heat transfer coefficient, σ is the Stefan-Boltzmann constant for radiation, ε_{rad} is the emissivity, T_0 denotes the nodal temperature and T_0 is the ambient temperature. On the boundary S for $(x,y,z) \in S$ and $t>0$. S represents those surfaces subjected to radiation, convection, and imposed heat fluxes.

4 FINITE ELEMENT (FE) MODEL DEVELOPMENT

A FE model of the laser-assisted Ti to polyimide Welding process has been developed by ABAQUS software to predict temperature field in the materials. The main advantage of the FE model is to anticipate the process parameters that ensures an appropriate polymer temperature, for the considered heat source power. The dissimilar joint can only be achieved if the polymer temperature is within melting point and degradation temperature. In this FE model Ti and Polyamide parts are meshed using coupled temperature-displacement elements to conduct thermal/mechanical analysis. A coupled temperature displacement transient analysis is a nonlinear simultaneous solution of temperature and displacement for thermomechanical problems, where displacement can be due to thermal effects and mechanical loading. The mesh pattern is also non-uniform to generate fine meshes along with laser travelling direction to predict accurate temperature distribution. The coarse meshes are used in other parts of the 3-D model as shown in Figure 3 to avoid high simulation time.

The verification of the FE model is achieved by series of refining tests for sizing mesh to explore the sensitivity of the model predictions towards the size of elements. The material properties of Ti and Polyamide used in the simulation are temperature dependent, provided in Table 1 and Table 2, and are obtained from the literature [28]. Radiation and natural convection have been considered for the heat transfer boundary condition at all sides open to surrounding. The time has been calculated based on the scanning speed and heat source location.

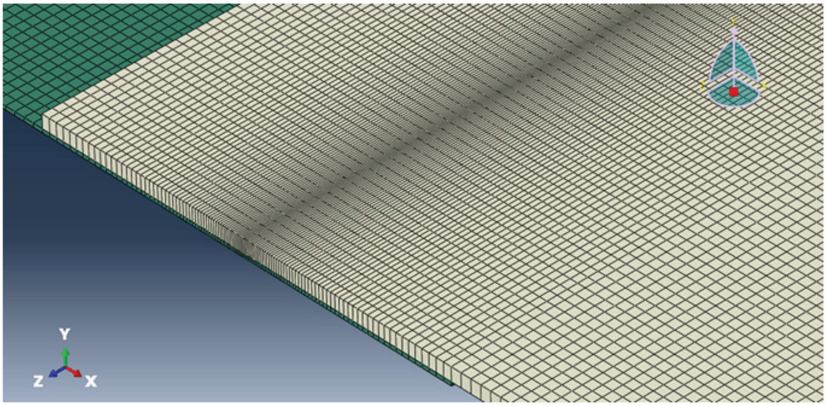

FIGURE 3
FE mesh of the joining parts.

TABLE 1
Ti material properties at different temperatures.

Temperature(°C)	27	100	200	300	400	500	600	700	800
Density (kg/m^3)	4500	-	-	-	-	-	-	-	4350
Poisson's ratio	0.32	0.32	0.32	0.32	0.32	0.32	0.32	0.32	0.32
Thermal conductivity (W/m C)	20.42	18.95	18.0	18.07	18.2	18.70	19.54	20.49	21.40
Specific heat (J/g C)	0.52	0.535	0.555	0.589	0.620	0.658	0.696	0.743	0.79
Coefficient of thermal expansion ($\times 10^{-6}$ °C^{-1})	4.92	-	-	-	-	-	-	-	5.62
Elastic modulus (GPa)	106	103	95.5	87	80	87	-	-	80
Yield stress (MPa) at strain (m/m) of 0.0	240	185	125	80	77	60	-	-	50
Yield stress (MPa) at strain (m/m) of 0.5	568	388	261	234	187	170	-	-	129

5 NUMERICAL ANALYSIS

5.1 Simulation

The Fortran program is linked to the ABAQUS software to simulate the laser welding process. Laser welding simulation is performed with the following process parameters: laser beam power, Q_L=1 W; scanning speed, v=100 mm/min; laser beam radius, r_0=100 μm; laser efficiency, η_L=85%; and the laser

TABLE 2
Polyimide material properties at different temperatures.

Temperature(°C)	27	50	100	150	200	250	300	350	400
Density (kg/m3)	1.43	-	-	-	-	-	-	-	1.40
Poisson's ratio	0.4	0.4	0.4	0.4	0.4	0.4	0.4	0.4	0.4
Thermal conductivity (W/m C)	0.174	0.175	0.175	0.176	0.177	0.178	0.178	0.179	0.18
Specific heat (J/g C)	1.000	1.002	1.004	1.110	1.200	1.325	1.423	1.450	1.470
Coefficient of thermal expansion ($\times 10^{-6}$ °C^{-1})	4.5	-	-	-	-	-	-	-	5.5
Elastic modulus (MPa)	2760	2350	1720	900	450	30	10	5	1.00
Yield stress (MPa) at strain (m/m) of 0.0	70	61	46	31	16	3.5	2	2	1.00
Yield stress (MPa) at strain (m/m) of 0.5	510.00	280.00	130.00	87.00	63.00	3.50	0.01	0.01	0.01

beam is at focus length on the Ti surface. The temperature distribution of the joining parts changes quickly with time and space during laser radiation.

Figure 4 shows the temperature profiles after the temperatures have been stabilized on the polyimide side transverse to the laser scanning direction. The highest temperature of this profile at the centre of the laser spot is lower than degradation point (around 500°C) of the polyimide and therefore the bond width can be predicted by the zone that has gained temperatures higher than melting point of the polyimide (350°C). The predicted bond width by temperature profile at the middle of laser travelling direction is 0.32 mm.

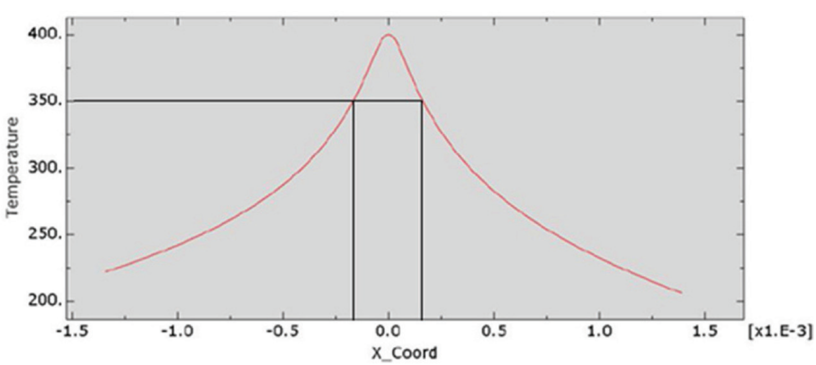

FIGURE 4
Temperature profile transverse to the laser scanning direction.

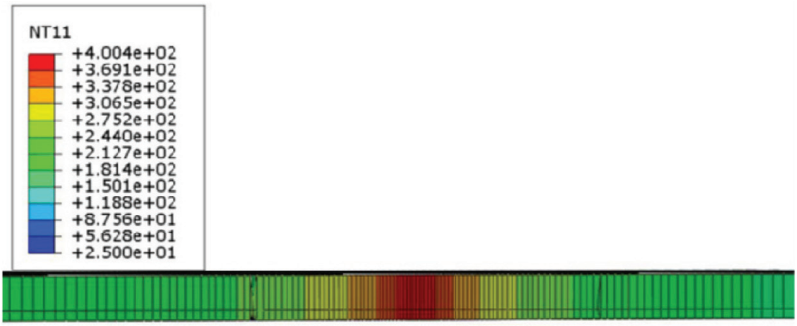

FIGURE 5
Temperature contours at *x-y* plane for a laser power of 1.00 W and a scanning speed of 100 mm/min with the laser beam focused onto the Ti surface.

Figure 5 also shows the temperature contours at *x-y* plane transverse to the laser scanning direction. It can also be revealed by results of the simulation that there is a slight increase in bond width along with laser travelling direction which is an indication of rising heat absorption by Ti along with laser travelling direction. The maximum bond width is at the end point and the minimum bond width is at the start point of laser travelling direction.

5.2 Experimental validation

A thermoplastic polyimide sheet (Imidex) was joined to Ti by means of continuous wave (CW) radiation from a Yb-doped fiber laser at a wavelength, λ=1.1 μm by Newaz *et al.* [23]. The transmission joining configuration shown in Figure 1 was employed in which a clamping pressure of 415 kPa was applied. A schematic diagram of the prepared Ti and polyimide sample is shown in Figure 6. The laser beam with a total power of 1.00 W was loosely

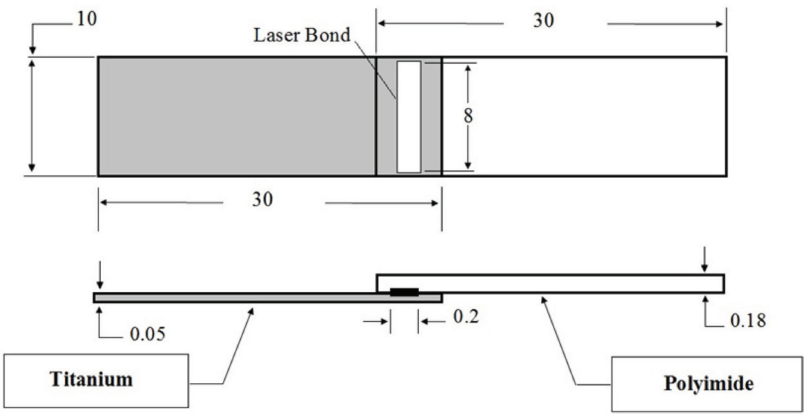

FIGURE 6
Schematic diagram of the Ti/polyimide tensile testing samples.

focused on the Ti surface to a spot with diameter 200 μm. A scanning speed of 100 mm/min was used to produce the 8 mm long joint line and a bond width of 0.3 mm was measured by an optical microscope (Binoc-2; AFM, Ltd.). The experimental bond width is in good agreement with the simulation result, hence the FE model is valid; therefore, the FE model can be used by RSM to evaluate effects of different process parameters on bond width.

6 RESPONSE SURFACE METHODOLOGY (RSM)

RSM allows an experimenter to explore functional relationships between a response variable and controlled variables. The main goals of RSM are to use a sequence of planned experiments to seek an optimal response and to evaluate a functional relationship in the neighbourhood of the optimal response [29]. A functional relationship relating a response η with the k levels of controlled variables is [30]

$$Y=f(X_1,X_2,X_3,\ldots X_n)\pm\varepsilon \tag{5}$$

where ε represents the random experimental error due to some unknown or uncontrollable variables. To optimize the response Y, it is necessary to find an appropriate approximation for the true functional relationship between the independent variables and the response surface [31]. The second order polynomial equation is used for representing the response and also expressed in the form

$$Y=\beta_0+\sum_{i=1}^{n}\beta_i X_i+\sum_{i=1}^{n}\beta_{ii} X_i^2+\sum_{i,j=1,i\neq j}^{n}\beta_{ij} X_i X_j+\varepsilon \tag{6}$$

In this study laser power, P, and laser scanning speed, S, are considered as input variables. Responses variables are average bond width and delta bond width. Average bond width is the average of maximum bond width at the end point and minimum bond width at the start point of laser travelling direction. Delta bond width is the difference between maximum and minimum bond width. The analysis is designed based on central composite design (CCD) full replication with two factors five levels. Table 3 shows levels of independent

TABLE 3
Levels of independent variables.

Variable	Symbol	Unit	Levels				
Laser power	P	W	0.50	0.75	1.00	1.25	1.50
Laser scanning speed	S	mm/min	50	75	100	125	150

TABLE 4
Design matrix and numerical results.

Run	Input Variables		Output Responses	
	Laser power (W)	Laser scanning speed (mm/min)	Average bond width (mm)	Delta bond width (mm)
1	1.00	100.00	0.33	0.06
2	1.00	100.00	0.33	0.06
3	1.00	100.00	0.33	0.06
4	1.00	100.00	0.33	0.06
5	1.25	125.00	0.35	0.07
6	1.25	75.00	0.48	0.08
7	0.75	75.00	0.3	0.18
8	1.50	100.00	0.49	0.05
9	1.00	50.00	0.44	0.30
10	1.00	150.00	0.28	0.03
11	0.50	100.00	0.16	0.05
12	0.75	125.00	0.12	0.02
13	1.00	100.00	0.33	0.06

variables. The designed experiments and results of the numerical simulation are shown in Table 4.

7 RESULTS AND DISCUSSION

7.1 General approach

Output responses are attained by FE predictions of maximum and minimum bond width at the end point and start point of laser travelling direction. Design-Expert V8 software is used to carry out statistical analysis. The analysis of variance (ANOVA) depicts effects of independent variables on the average bond width and delta bond width. The ANOVA is built entirely on the premise that the factors are fixed, not random and the design is crossed, not nested. The model F-Values imply the models are significant. Values of Prob>F less than 0.0500 indicate model terms are significant. The results confirm that models are significant and these models can be used to navigate the design space. In the mathematical model the software selects the higher polynomial where the additional terms are significant and the model is not aliased.

7.2 Average bond width

The F Value of ANOVA table indicates that laser power and laser scanning speed are the most significant controlled variables for average bond width. Table 5 demonstrates ANOVA analysis for average bond width.

The final equation of average bond width and in terms of actual factors is

$$(w\ average)^{1.6} = 0.27465 + 0.27904P - 5.66054 \times 10^{-3} + (1.80855 \times 10^{-5})^2 \tag{7}$$

Figure 7 depicts perturbation plot of average bond width. Line A shows sensitivity of average bond width to laser power and Line B shows sensitivity of average bond width to laser scanning speed. The perturbation plot depicts that increasing laser power leads to wider bond width however, increasing laser scanning speed results in narrower bond width.

In order to gain a suitable understanding of laser welding process the heat input concept is defined. Heat input, H_i, can be explained by [32]

$$H_i = \frac{Q_L}{v} \tag{8}$$

Results indicate that there is a direct relationship between heat input and average bond width. It can be revealed that increasing laser power at lower laser scanning speed leads to higher heat input which results in larger average bond width; in fact, increasing heat input leads to higher heat absorption by the metal surface which results in larger bond width.

TABLE 5
Analysis of variance (ANOVA) for average bond width.

Source	Sum of Squares	df	Mean Square	F Value	p-value Prob>F
Model	0.093	3	0.031	128.23	< 0.0001
P	0.058	1	0.058	241.82	< 0.0001
S	0.031	1	0.031	129.68	< 0.0001
S^2	3.184×10^{-3}	1	3.184×10^{-3}	13.19	0.0055
Residual	2.173×10^{-3}	9	2.415×10^{-4}	128.23	< 0.0001
Lack of Fit	2.173×10^{-3}	5	4.347×10^{-4}		
Pure Error	0.000	4	0.000		
Cor Total	0.095	12			
	Adj R-Squared	0.9695	R-Squared	0.9771	

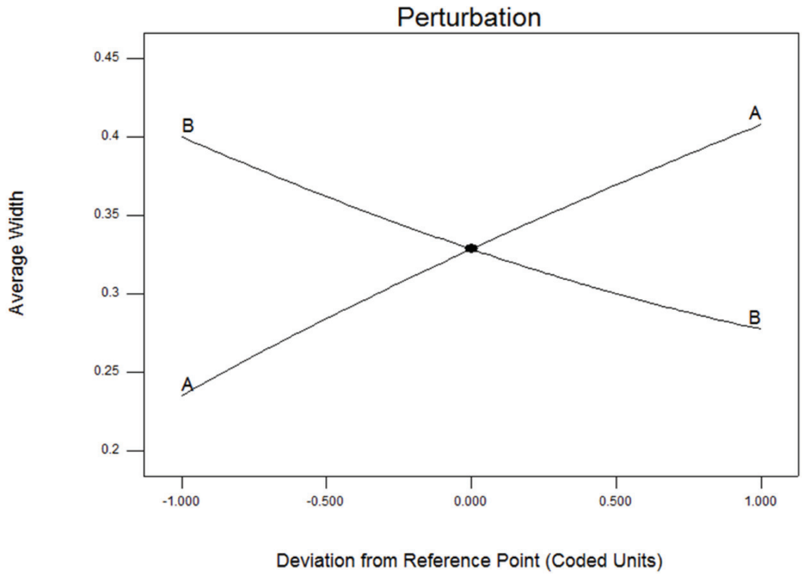

FIGURE 7
Perturbation plot of average bond width.

7.3 Delta bond width

The F Value of ANOVA table demonstrates laser scanning speed and the interaction between laser power and laser scanning speed are the most influential parameters on delta bond width. Table 6 demonstrate ANOVA analysis for delta bond width.

The final equation of the delta bond width in terms of actual factors is

$$(\mathit{Delta\ w})^{0.33}=2.26592 - 1.04019P - 0.023650S + 0.012193PS - 0.081581P^2 + (3.97747 \times 10^{-5})^2 \tag{9}$$

Figure 8 depicts perturbation plot of the delta bond width. The perturbation plot shows that increasing laser scanning speed leads to smaller delta bond width. In addition, the interaction between laser scanning speed and laser power has an important impact on delta bond width. The perturbation plot indicates that laser power has little effect on delta bond width; moreover, increasing laser scanning speed at lower laser power results in lower heat input which leads to smaller delta bond width.

7.4 Numerical optimization

In this numerical optimization two criteria are implemented. The objective of the first optimization criterion is to attain maximum average bond width with minimum delta bond width. Wider bond width can result in higher strength in

TABLE 6
Analysis of variance (ANOVA) for delta bond width.

Source	Sum of Squares	df	Mean Square	F Value	p-value Prob>F
Model	0.13	5	0.027	509.92	<0.0001
P	1.909×10^{-4}	1	1.909×10^{-4}	3.65	0.0976
S	0.092	1	0.092	1760.03	<0.0001
PS	0.023	1	0.023	444.49	<0.0001
P^2	5.957×10^{-4}	1	5.957×10^{-4}	11.40	0.0118
S^2	0.014	1	0.014	270.95	<0.0001
Residual	3.658×10^{-4}	7	5.226×10^{-5}		
Lack of Fit	3.658×10^{-4}	3	1.219×10^{-4}		
Pure Error	0.000	4	0.000		
Cor Total	0.13	12			
	Adj R-Squared	0.9953	R-Squared	0.9973	

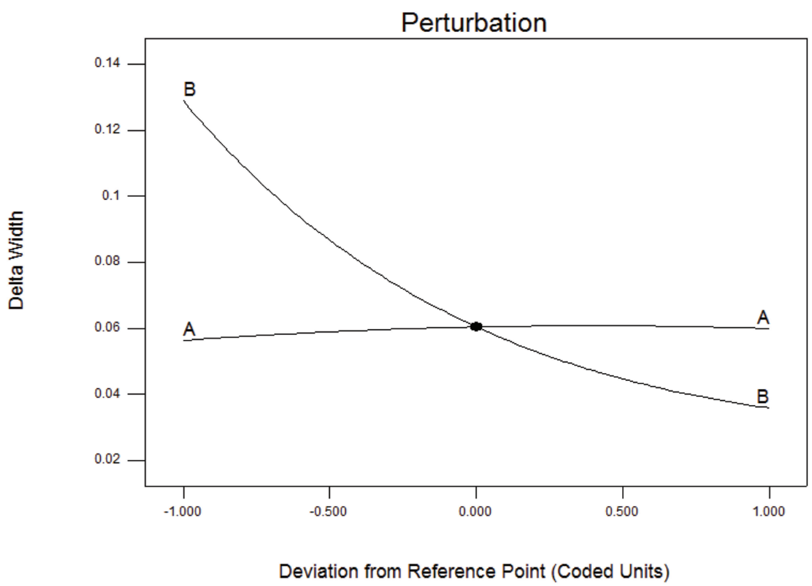

FIGURE 8
Perturbation plot of delta bond width.

the dissimilar joint and also non-uniform bond width along with the joint can lead to unbalanced resistance against loading condition; in fact, joint strength is affected by average bond width but, a joint with a uniform bond width along with the joint line is more resistant to loading than a joint with the same average width but larger delta width. Table 7 shows the first criterion of numerical optimization.

The objective of the second optimization criterion is to attain maximum average bond with maximum laser scanning speed. In some parts, the joint can be produced by several joining lines between joining parts. Higher laser scanning speed is favourable in the joints with several joining lines to reduce overall production time. Table 8 shows the second criterion of numerical optimization. The optimized process parameters to achieve the first and second optimization criterion are shown in Table 9 and Table 10, respectively. All

TABLE 7
The first criterion of numerical optimization.

Name	**Goal**	**Lower limit**	**Upper limit**	**Lower Weight**	**Upper Weight**	**Importance**
Laser power	Is in range	0.75	1.25	1	1	3
Laser scanning speed	Is in range	75	125	1	1	3
Average bond width	Maximum	0.117	0.486	1	1	3
Delta bond width	Minimum	0.05	0.20	1	1	3

TABLE 8
The second criterion of numerical optimization.

Name	**Goal**	**Lower limit**	**Upper limit**	**Lower Weight**	**Upper Weight**	**Importance**
Laser power	Is in range	0.75	1.25	1	1	3
Laser scanning speed	Maximum	75	125	1	1	3
Average bond width	Maximum	0.117	0.486	1	1	3
Delta bond width	Is in range	0.015	0.303	1	1	3

TABLE 9
Optimized process parameters to achieve the first optimization criterion.

Number	**Power**	**Speed**	**Average Width**	**Delta Width**	**Desirability**
1	1.25	80.48	0.456354	0.0716997	0.887
2	1.25	80.24	0.457011	0.0719495	0.887
3	1.25	80.76	0.455591	0.071413	0.887

TABLE 10
Optimized process parameters to achieve the second optimization criterion.

Number	Power	Speed	Average Width	Delta Width	Desirability
1	1.25	125.00	0.363957	0.0663942	0.818
2	1.25	124.81	0.3642	0.0662543	0.817
3	1.24	125.00	0.359382	0.064441	0.810

optimum solutions take advantage of the high level of desirability. The solutions of the first optimization criterion indicate higher laser power and relatively high laser scanning speed lead to joint with maximum average width and minimum delta width.

In comparison, the solutions of the second optimization criterion reveal higher speed needed to reduce joining time leads to lower average width and smaller delta width. Figure 9 depicts the numerical optimization graphs to demonstrate interaction effects of input variables on output responses. The two-dimensional (2-D) contour graphs have a flag planted at the No. 3 optimum point of the first optimization criterion. It can be useful to see how a single response behaves in the vicinity of a particular optimum. Figure 10 shows overlay plot which is comprised of the contour plots from each response laid on top of each other. On each contour plot, the undesirable area is greyed-out. The yellow area that remains defines the final optimal factor settings [33, 34].

8 CONCLUSIONS

In this paper a numerical and statistical analysis of laser-assisted Ti to polyimide has been carried out. The finite element (FE) model was developed by ABAQUS software to evaluate thermal phenomena of the laser welding process. The cylindrical-involution-normal (CIN) heat source model was used to approximate heat source distribution. The Fortran program was linked to ABAQUS to simulate laser-assisted Ti to polyimide welding. The FE model was verified by series of refining tests and then validated by results of the experimental data. It could be observed that bond width predicted by FE model (0.32 mm) was similar with the experimental bond width measured by an optical microscope (0.3 mm). Thereafter, the validated FE model was used by response surface methodology (RSM) to predict bond width for designed experiments. Effects of laser power and laser scanning speed on average bond width and delta bond investigated by analysis of variance (ANOVA). Results show that increasing heat input results in wider bond. Decreasing heat input, however, leads to less variation in bond width along with laser travelling

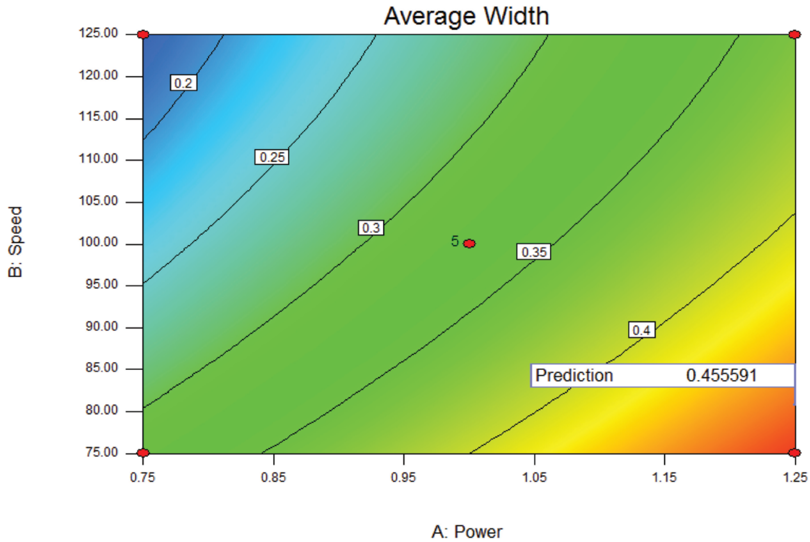

(a)

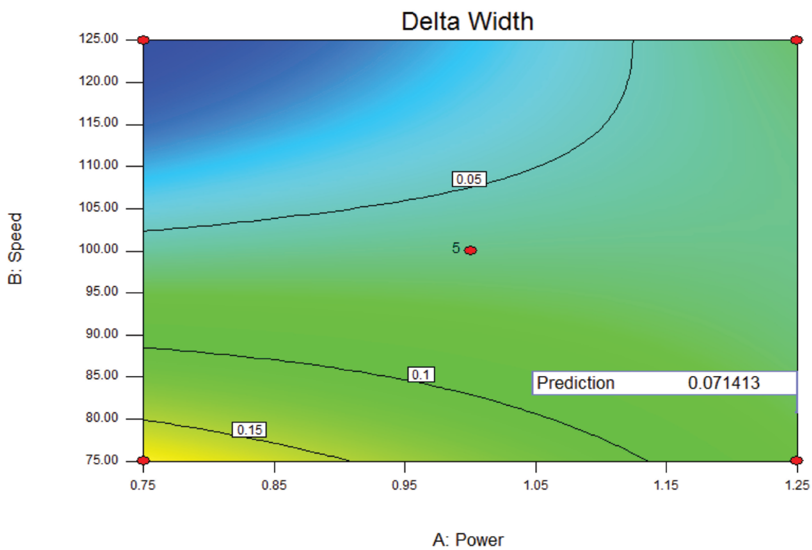

(b)

FIGURE 9
Numerical optimization graphs for response variables for (a) average width and (b) delta width.

direction. The solutions of the first optimization criterion are suggested to join parts by a joining line. While, the solutions of the second optimization criterion are suggested to join parts by several joining lines. The obtained setting of optimum process parameters for the first optimization criterion

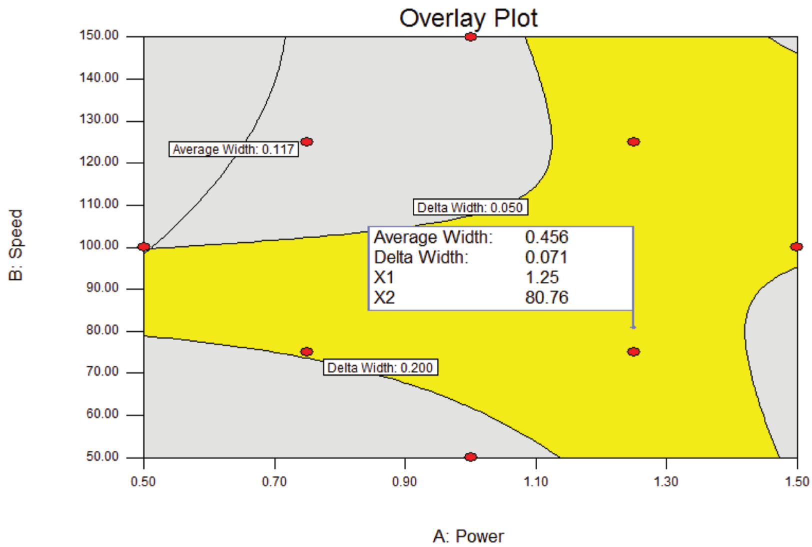

FIGURE 10
Overlay contour plot.

are laser power of 1.25 W and laser scanning speed of 80.48 mm/min. The obtained setting of optimum process parameters for the second optimization criterion are laser power of 1.25 W and laser scanning speed of 125.0 mm/min.

NOMENCLATURE

c	Specific heat capacity (J/kgK)
h_{conv}	Convection heat transfer coefficient (W/m^2 K)
H_i	Heat input (J/m)
k	Beam focus coefficient
kn	Thermal conductivities (W/mK)
K_Z	Heat source power exponent
P	Laser power (W)
q	Heat flux (W/m^2)
Q	Heat generation rate in *per* unit volume (W/mK)
Q_L	Laser beam power (W)
r_0	Beam radius (m)
s	Heat source beam penetration depth (m)
S	Laser scanning speed (mm/min)
t	Time (seconds)
T	Temperature (K)
T_0	Ambient temperature (K)
v	Velocity of the laser beam across the surface (m/s)

Greek symbols

ε Random experimental error
η_L Laser efficiency
ρ Material density (kg/m^3)
σ Stefan-Boltzmann constant (5.67×10^{-8} W/m^2K^4)

REFERENCES

[1] Roesner A., Scheik S., Olowinsky A., Gillnera A., Reisgen U. and Schleser M. Laser assisted joining of plastic metal hybrids. *Physics Procedia* **12** (2011), 370–377.

[2] Moradi M., Mehrabi O., Azdast T. and Benyounis K.Y. The effect of low power CO_2 laser cutting process parameters on polycarbonate cut quality produced by injection molding. *Modares Mechanical Engineering* **17**(2) (2017), 93–100.

[3] Moradi M., Mohazab A. and Khorram A. An experimental investigation of the effects of fiber laser percussion drilling: Influence of process parameters. *International Journal of Advanced Design and Manufacturing Technology* **9**(4) (2016), 7–12.

[4] Faraji A.H., Moradi M., Goodarzi M., Colucci P. and Maletta C. An investigation on capability of hybrid Nd:YAG laser-TIG welding technology for AA2198 Al-Li alloy. *Optics and Lasers in Engineering* **96** (2017), 1–6.

[5] Moradi M., Ghoreishi M., and Khorram A. Process and outcome comparison between laser, tungsten inert gas (TIG) and laser-TIG hybrid welding. *Lasers in Engineering* **39**(1–4) (2018), 77–99

[6] Khorram A., Jafari A. and Moradi M. Laser brazing of 321 and 410 stainless steels using BNi-2 nickel-based filler metal. *Modares Mechanical Engineering* **17**(1) (2017), 129–135.

[7] Katayama S., Kawahito Y. and Mizutani M. Latest progress in performance and understanding of laser welding. *Physics Procedia* **39** (2012), 8–16.

[8] Meiabadi M.S., Kazerooni A. and Moradi M. A brief review: Laser assisted metal to polymer welding. *2nd National Conference on Modern Approaches in Mechanical Engineering.* 7 September 2017, Malayer, Iran. pp. 25–34.

[9] Bauernhuber A. and Markovits T. Investigating thermal interactions in the case of laser assisted joining of PMMA plastic and steel. *Physics Procedia* **56** (2014), 811–817.

[10] Katayama S. and Kawahito Y. Laser direct joining of metal and plastic. *Scripta Materialia* **59** (2008), 1247–1250.

[11] Dhorajiya A.P., Mayeed M.S., Auner G.W., Baird R.J, Newaz G.M., Patwa R. and Herfurth H. Finite element thermal/mechanical analysis of transmission laser microjoining of titanium and polyimide. *Journal of Engineering Materials and Technology* **132**(1) (2010), 011004

[12] Wahbaa M., Kawahitoc Y. and Katayama S. Laser direct joining of AZ91D thixomolded Mg alloy and amorphous polyethylene terephthalate. *Journal of Materials Processing Technology* **211** (2011), 1166–1174.

[13] Hino M., Mitooka Y., Murakami K., Urakami K., Nagase. H and Kanadani T. Effect of aluminum surface state on laser joining between 1050 aluminum sheet and polypropylene resin sheet using insert materials. *Materials Transactions* **52** (2011), 1041–1047.

[14] Kawahito Y., Nishimoto K. and Katayama S. LAMP joining between ceramic and plastic. *Physics Procedia* **12** (2011), 174–178.

[15] Roesner A., Scheik S., Olowinsky A., Gillner A., Reisgen U. and Schleser M. Laser assisted joining of plastic metal hybrids. *Physics Procedia* **12** (2011), 370–377.

[16] Sano T., Iwasaki S., Ozeki Y., Itoh K. and Hirose A. Femtosecond laser direct joining of copper with polyethylene terephthalate. *Materials Transactions* **54**(6) (2013), 926–930.

[17] Heckert A. and Zaeh M.F. Laser surface pre-treatment of aluminium for hybrid joints with glass fibre reinforced thermoplastics. *Physics Procedia* **56** (2014), 1171–1181.

[18] Markovits T. and Bauernhuber A. Comparing adhesive bonding and LAMP joining technology in case of hybrid material combination. *Physics Procedia* **56** (2014), 818–823.

[19] Lamberti C., Solchenbach T., Plapper P. and Possart W. Laser assisted joining of hybrid polyamide-aluminum structures. *Physics Procedia* **56** (2014), 845–853.

[20] Vidal E.R., Lambarri J., Soriano C., Sanz C. and Verhaeghe G. A combined experimental and numerical approach to the laser joining of hybrid polymer-metal parts. *Physics Procedia* **56** (2014), 835–844.

[21] Schricker k., Stambke M. and Bergmann J.P. Experimental investigations and modeling of the melting layer in polymer-metal hybrid structures. *Weld World* **59** (2015), 407–412.

[22] Cenigaonaindia A., Liébana F., Lamikiz A. and Echegoyen Z. Novel strategies for laser joining of polyamide and AISI 304. *Physics Procedia* **39** (2012), 92–99.

[23] Newaz G., Mian A., Sultana T., Mahmood T., Georgiev D.G., Auner G., Witte R. and Herfurth H. A comparison between glass/polyimide and titanium/polyimide microjoint performances in cerebrospinal fluid. *Journal of Biomedical Materials Research* **79**(1) (2006), 159–65.

[24] Kubiak M., Piekarska W. and Parkitny R. Theoretical study on thermal and structural phenomena in thin elements heated by a laser beam. *Archives of Mechanics* **67**(1) (2015), 3–24.

[25] Mościcki T., Hoffman J. and Szymański Z. Modelling of plasma formation during nanosecond laser ablation. *Archives of Mechanics* **63**(2) (2011), 99–116.

[26] Piekarska W., Kubiak W., Saternus M. and Saternus Z. Computer simulation of temperature field in laser beam welded lap joint. *Archives of Mechanical Technology and Automation* **32**(1) (2012), 37–45.

[27] Ranatowski E. Thermal modelling of laser welding. Part I: The physical basis of laser welding. *Advances in Materials Science* **1** (2003), 34–40.

[28] Mayeed M.S., Lubna N.J., Auner G.W., Patwa R., Herfurth H. and Newaz G.M. Finite element thermal/mechanical analysis for microscale laser joining of ultrathin coatings of titanium on glass/polyimide system. *Materials: Design and Applications* **225** (2011), 245–254.

[29] Moradi M. and Golchin E. Investigation on the effects of process parameters on laser percussion drilling using finite element methodology: Statistical modelling and optimization. *Latin American Journal of Solids and Structures* **14**(3) (2017), 464–484.

[30] Moradi M. and Mohazabpak A. Statistical modelling and optimization of laser percussion micro-drilling on Inconel 718 sheet using response surface methodology. *Lasers in Engineering* **40**(1–3) (2018), 156–167.

[31] Azadi M, Azadi S., Moradi M and Zahedi F. Multidisciplinary optimisation of a car component under NVH and weight constraints using RSM. *International Journal of Vehicle Noise and Vibration* **5**(3) (2009), 261–270.

[32] Moradi M., Mehrabi O., Azdast T. and Benyounis K.Y. Enhancement of low power CO2 laser cutting process for injection moulded polycarbonate. *Optics & Laser Technology* **96** (2017), 208–218.

[33] Benyounis K.Y, Olabi A.G. and Hashmi M.S.J. Optimizing the laser-welded butt joints of medium carbon steel using RSM. *Journal of Materials Processing Technology* **164–165** (2005), 986–989.

[34] Benyounis K.Y., Olabi A.G. and Hashmi M.S.J. Multi-response optimization of CO2 laser-welding process of austenitic stainless steel. *Optics & Laser Technology* **40**(1) (2008), 76–87.